Asian Journal of Chemistry; Vol. 25, No. 16 (2013), 8887-8891

ASIAN JOURNAL OF CHEMISTRY

http://dx.doi.org/10.14233/ajchem.2013.14894

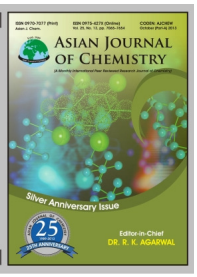

Nano-sized Fe-Metal Catalyst on TiO_2-SiO_2: (Photo-assisted Deposition and Impregnation) Synthesis Routes and Nanostructure Characterization

R.M. MOHAMED[1,2,*] and ELHAM S. AAZAM[1]

[1]Chemistry Department, Faculty of Science, King Abdul Aziz University, Jeddah, Kingdom of Saudi Arabia
[2]Nanostructured Material Division Advanced Materials Department, Central Metallurgical R&D Institute, Helwan 11421, Cairo, Egypt

*Corresponding author: Fax: +966 2 6952292; Tel: +966 5 40715648; E-mail: redama123@yahoo.com

(*Received*: 3 December 2012; *Accepted*: 5 September 2013) AJC-14073

The photo-assisted deposition and impregnation synthesis of nano-sized Fe metal on TiO_2-SiO_2 are reported. The prepared catalysts were characterized by different techniques such as XRD, XAFS, TEM and nitrogen adsorption analysis. Photocatalytic reactivity using Fe-TiO_2-SiO_2 catalysts under visible-light condition on the reduction of Hg^{2+} to Hg^0 was evaluated. The results have shown notable photocatalytic activity of photo-assisted deposition of Fe/TiO_2-SiO_2 which was 2 and 10 times higher than that of impregnation synthesis of Fe/TiO_2-SiO_2 and TiO_2-SiO_2, respectively.

Key Words: Visible photocatalyst, Fe-doped titania-silica, Hg^{2+}.

INTRODUCTION

Mercury(II) is a frequent component of industrial wastewaters and is used in agricultural applications such as pesticides, fungicides, herbicides, insecticides and bactericides, which are currently forbidden. Mercury is also used in other industries (*e.g.*, chlorine-alkali, paints, pharmaceuticals, electronics, cosmetics, *etc.*)[1,2]. In aquatic systems, mercury is often converted by bacteria into methyl mercury, being magnified hundreds to thousands of times as it moves through the aquatic food chain, posing a potential risk to humans and wildlife that consume fish[3]. Heterogeneous photocatalysis is a convenient tool for mercury reduction because it uses inexpensive chemicals[4]. TiO_2 photocatalysis is a much appreciated in recent years for environmental improvement such as the photodegradation and complete mineralization of organic pollutants[5,6]. TiO_2 nanoparticles have large specific surface areas and high catalytic performance in which reactions take place on the TiO_2 surface. However, their effective commercial applications are hindered by three serious disadvantages. Firstly, agglomerations of ultrafine powders into larger particles result in an adverse effect on catalyst performance. Secondly, the separation and recovery of TiO_2 powders from wastewater are complicated[7,8]. Thirdly, the requirements of ultraviolet radiation for TiO_2 photocatalysis performance whose energy exceeds the band gap of 3.2 eV (λ-380 nm) of the anatase crystalline phase, which in turn led utilization only a very small fraction of sunlight.

More recently, TiO_2 has attracted the attention of scientists in the catalysis field, due to its effective utilization of visible light to degrade organic pollutants. A considerable effort has been devoted to develop supported titania catalysts offering high active surface area, while at the same time having easier separation and removal from wastewater[9,10]. New synthesis methods of titania-silica mixed oxides are needed for overcoming the present disadvantages of pure titania powders. One of the ways is the use of charge-transfer catalysts, which can improve the efficiency of TiO_2. This type can be obtained by the preparation of TiO_2-SiO_2 catalyst with the electron transfer across the solid-solid TiO_2-SiO_2 interface. For that reasons, in a previous study it was reported that the TiO_2-SiO_2 catalyst is 3 times more photoactive than TiO_2 alone[11-13]. Another possibility is to modify TiO_2 by surface deposition of noble metals to shift the process of photodegradation of organic pollutants into the visible -light region[14-17].

Recently, there is much interest in a new nano-sized catalyst such as Pd, Pt and Au as potentially advanced materials possessing unique electronic, optic and magnetic properties as well as catalytic functions[18-21]. One of the most important factors for controlling catalytic activity of these metal catalysts is the particle size. The development of convenient and useful method to prepare the nano-sized metal loaded on support with controlled particle size and size distribution is an essential task to design a highly active metal catalyst.

Under UV-light irradiation, these single-site photocatalysts generate charge transfer excited state which can show the

highly active and selective photocatalytic performances. In previous studies[22-31], the main focus has been made only on the photocatalytic reactivity but the applications of single-site photocatalyst for the synthesis of conventional catalysts such as nano-sized metal catalyst have not been yet reported. It can be expected that the metal precursor species can be easily deposited on the excited state of single-site photocatalyst to form well-controlled sized metal particles from the mixture of single-site photocatalyst in the aqueous solution with metal precursor.

In the present study, Fe/TiO_2-SiO_2 was prepared by the application of a photo-assisted deposition (PAD) and impregnation methods. We focus on the photocatalytic reactivity of Fe/TiO_2-SiO_2 under visible- light for the reduction of Hg^{2+} to Hg^0.

EXPERIMENTAL

All chemicals are analytical grade reagents and used without further purification. The titania sol was prepared *via* acid peptizing the precipitate of titanium tetrachloride solution ($TiCl_4$) with ammonia solution. In a typical synthesis procedure, a 10 % NH_4OH was dropped into 20 mL $TiCl_4$ (0.18 mol) solution until a white precipitate is obtained at a pH = 7. The precipitate was washed with deionized water to remove the excess Cl^- and NH_4^+ ions. Afterward, about 25 mL of deionized water was added to form a suspension. By adding a calculated amount of 1.6 M HNO_3 ($[H^+]/[Ti]$ = 0.5 with strong stirring for 24 h at 70 ºC, the precipitate was peptized to form a highly dispersed and stable titania sol. Appropriate amount (6 mL) of tetraethyl orthosilicate (TEOS) 98 % $Si(OC_2H_5)_4$ solution was dropped into the above titania sol. The modified sol was dried and calcined at 400 ºC for 3 h to obtain SiO_2-TiO_2 catalyst. The content of SiO_2 in the modified catalyst was 10 wt. %

On the other side, the Fe loaded on TiO_2-SiO_2 (PAD-Fe/TiO_2-SiO_2, 5 wt % as Fe metal) was prepared using the photo-assisted deposition (PAD) method: Fe metal was deposited on TiO_2-SiO_2 from aqueous solution of ferric nitrate monohydrate under UV-light irradiation. The Fe loaded on TiO_2-SiO_2 (img-Fe/TiO_2-SiO_2, 5 wt % as Fe metal) was prepared using impregnation method. The Fe metal was deposited by a simple impregnation of TiO_2-SiO_2 in the absence of light with aqueous solution of ferric nitrate monohydrate. The samples were dried at 378 K and reduced by H_2 (20 mL min^{-1}) at 473 K for 2 h.

Characterization techniques: The structure of the catalyst was examined by X-ray diffraction on a Rigaku X-ray diffractometer system equipped with as RINT 2000 wide angle Goniometer using CuK_α radiation and a power of 40 kV × 30 mA. The intensity data were collected at 25 ºC over a 2θ range of 20-80º. The UV-visible diffuse reflectance absorption spectra were recorded with a Shimadzu UV-2450 at 295 K. The X-ray absorption fine structure (XAFS) analysis, X-ray absorption near edge structure (XANES) and extended X-ray absorption fine structure (EXAFS), were performed. A Si(111) double crystal was used to monochromatize the X-rays from the 2.5 GeV electron storage ring. The K-edge XAFS spectra of Fe was measured in the fluorescence mode at 298 K.Fourier transformed was performed on κ^3-weighted EXAFS oscillations in the range of 1-10 $Å^{-1}$. N_2-adsorption measurement was carried out at 77 K using Nova 2000 series, Chromatech. Prior to analysis, the samples were outgased at 250 ºC for 4 h. The morphology and particle size of the prepared samples were examined *via* a transmission electron microscope (Hitachi H-9500 operated at 300 kv).

Photocatalytic experiment

Photoreduction: Stock solutions of Hg(II) (120 mg mL^{-1}) were prepared from a Merck (99.5 %) $HgCl_2$ solution in water. The reaction mixture was kept in a reactor with a cylindrical Pyrex cell of 1000 cm^3 and 500 cm^3 of a Hg(II) solution of a given concentration was added to 1 g of the photocatalyst. The solution pH was adjusted to 4 with formic acid. The reaction was conducted with the reactor open to air and oxygen stream bubbled in the suspension at 0.5 cm^3/min. A 125-W medium pressure mercury lamp with UV cut filter, surrounded by a quartz thimble, was used for irradiation. In order to maintain the room temperature (20 ºC), the vessel was surrounded by a water jacket with an inlet and an outlet for the passage of cold water. The reactor contained a magnetic stirrer to maintain the reaction mixture homogeneous. At regular intervals, 6 cm^3 aliquots of the suspension were withdrawn and filtered through a 0.45-µm Millipore filter. The concentration of mercury(II) in solution was determined by a Spectra AA-10 Plus VARIAN spectrophotometer.

The photocatalytic reduction efficiency of Hg^{2+} was estimated by applying the following equation:

$$\% \text{ Photocatalytic reduction of } Hg^{2+} = (C_o - C)/C_o \times 100$$

where C_o is initial concentration of Hg^{2+} and C is the residual Hg^{2+} concentration in solution.

Adsorption: In order to verify the adsorption capacity, experiments without a mercury lamp and formic acid were developed. The reaction mixture was kept in a reactor with a cylindrical Pyrex cell in 1000 cm^3 of water; 500 cm^3 of a Hg(II) solution of a given concentration was added to 1 g of the photocatalyst. The reactor was open and an air and oxygen stream was bubbled in the suspension at 0.5 cm^3/min. The reactor contained a magnetic stirrer to maintain the homogeneity of the reaction mixture. At regular intervals, a 6 cm^3 aliquot of the suspension was withdrawn and filtered through a 0.45 µm Millipore filter. The concentration of Hg(II) in the solution was determined by a spectra AA-10 Plus VARIAN spectrophotometer, which was used for all spectrophotometric measurements (wavelength 253.7).

The adsorption efficiency of Hg^{2+} was estimated by applying the following equation:

$$\% \text{ adsorption efficiency of } Hg^{2+} = (C_o - C)/C_o \times 100$$

where C_o is initial concentration of Hg^{2+} and C is the residual Hg^{2+} concentration in solution.

RESULTS AND DISCUSSION

XRD analysis: XRD patterns of each parent TiO_2-SiO_2 and Fe-doped TiO_2-SiO_2 nanoparticles prepared by impregnation method and photo-assisted deposition method are compared (Fig. 1). The structural characteristic of TiO_2-SiO_2 and all Fe-doped TiO_2-SiO_2, are mainly composed of anatase phase containing a group of lines at 2θ values of 25.2, 37.5, 47.7, 53.3, 54.7 and 62º [PDF # 71-1169], which indicated

that, titania anatase phase structure was remained after the application of the photo-assisted deposition and impregnation methods. However, no diffraction peaks of Fe in the patterns of Fe-doped samples were surveilled. This is probably attributed to the low Fe doping content (5 %). Moreover, the data may imply that, the Fe is well dispersed within the TiO_2-SiO_2 phase.

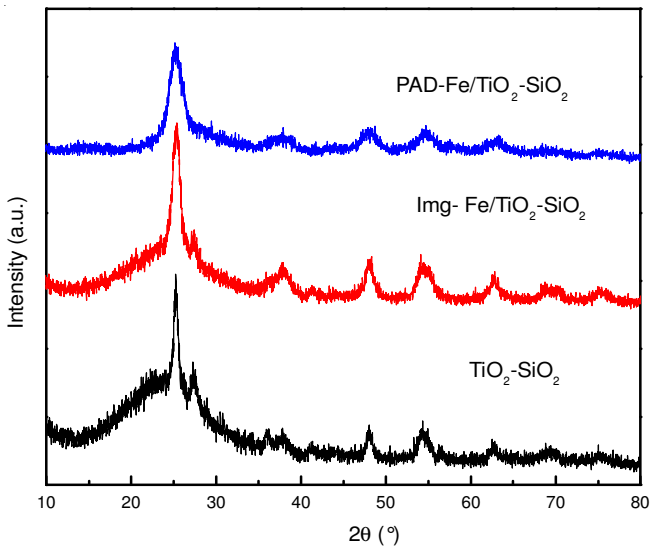

Fig. 1. XRD patterns of the TiO_2-SiO_2, PAD-Fe/TiO_2-SiO_2 and img-Fe/ TiO_2-SiO_2

UV-visible spectroscopy: Fig. 2 depicts the diffuse reflectance UV-visible absorption spectra of TiO_2-SiO_2, PAD-Fe/TiO_2-SiO_2 and imp-Fe/TiO_2-SiO_2. The Kubelka-Munk function, F(R), can be considered to be proportional to the absorption of radiation. On this basis, the value of E_g, the band gap of the semiconductor, can be derived from the spectra by plotting $[F(R).h\nu]^{1/2}$ against hν as shown in Fig. 3[32]. The band-gap values usually reported for pure anatase and rutile phases are 3.2 and 3.03 eV, respectively[33]. However, these values are influenced by the synthesis method and also affected by the existence of impurities doping the crystalline network and also the average crystal size of the semiconductor. In a previous study, different methods for calculating the E_g from the UV-visible reflectance spectra are used. For example, some authors calculate the E_g values by a direct extrapolation of the F(R) spectrum whereas others report the wavelength corresponding to the maximum absorption[34]. As a consequence, quite different E_g values for rutile and anatase samples are found in the literature. For instance, for anatase-based materials the threshold wavelength values of 370 nm[35], 380 nm[36], 387 nm[37], 393 nm[38] and 403 nm has been reported[39] corresponding to a band gap range from 3.08 to 3.35 eV have been reported. In the case of rutile-based materials, an absorption wavelength as high as 437.4 nm (E_g = 2.84 eV)[40]. In the present study, the band gap values calculated for TiO_2-SiO_2, PAD-Fe/TiO_2-SiO_2 and Img-Fe/TiO_2-SiO_2 are 3.20, 2.84 and 2.54 eV, respectively. Therefore, the study of UV-visible radiation absorption constitutes an important tool for the evaluation of the changes produced in the semiconductor materials by different treatments.

Specific surface area trends: The surface area changed from 300 (parent TiO_2-SiO_2) to 280 and 260 m^2/g in case of PAD-Fe/ TiO_2-SiO_2 and Img-Fe/ TiO_2-SiO_2 respectively (Table-1).

TABLE-1
BET SURFACE AREA OF TiO_2-SiO_2, PAD-Fe/TiO_2-SiO_2 AND Img- PAD-Fe/TiO_2-SiO_2

Sample	S_{BET} (m^2/g)
TiO_2-SiO_2	300
PAD-Fe/ TiO_2-SiO_2	280
Img- PAD-Fe/ TiO_2-SiO_2	260

Note: (S_{BET}) BET-surface area

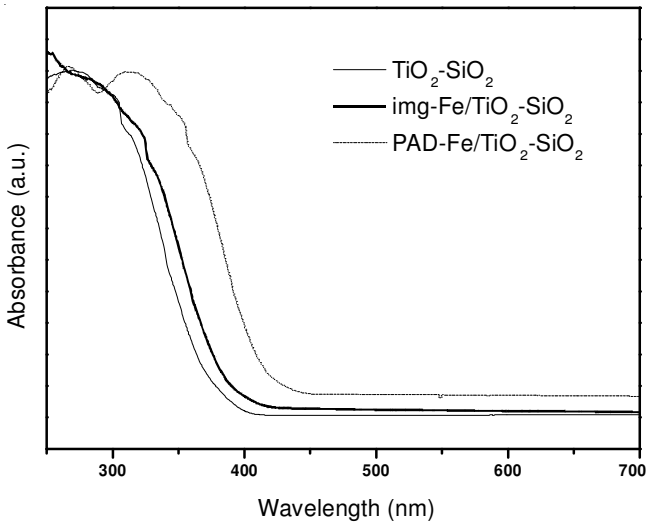

Fig. 2. Diffuse reflectance UV-visible absorption spectra of TiO_2-SiO_2, PAD-Fe/TiO_2-SiO_2 and img/Fe-TiO_2-SiO_2

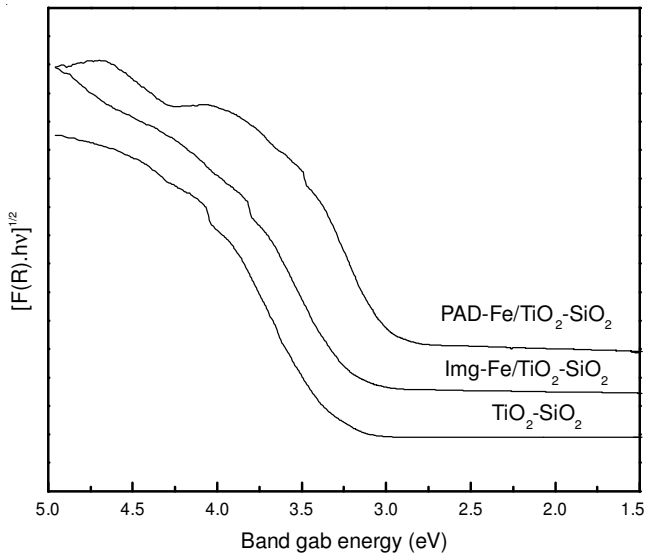

Fig. 3. Band-gap calculated from the DR-UV-visible spectra

EXAFS analysis: The Fourier transforms of Fe LIII-edge EXAFS spectra of the Fe-loaded catalysts are shown in Fig. 4. The presence of the peak assigned to the Fe-Fe bond at around 2.50 Å indicates the formation of nano-sized Fe metal. The intensity of the Fe-Fe peak of the PAD-Fe/TiO_2-SiO_2 catalyst is smaller than the img-Fe/TiO_2-SiO_2 catalyst. These findings suggest that the size of Fe metal particles depends on the preparation

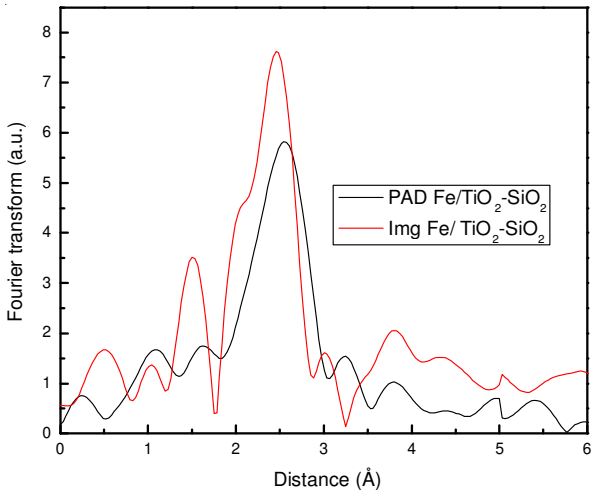

Fig. 4. Fourier transforms of the Fe LIII-edge EXAFS spectra for img-Fe/TiO_2-SiO_2 and PAD-Fe/TiO_2-SiO_2

method. Fe metal particles formed on the photo-deposited catalyst (PAD-Fe/TiO_2-SiO_2) show smaller particle size than that of the impregnated catalyst (img-Fe/TiO_2-SiO_2). Also, we can control the size of the Fe particles by varying content of Ti oxide, light intensity and light wavelength.

TEM Observation: The TEM images of PAD-Fe/TiO_2-SiO_2 and img-Fe/TiO_2-SiO_2 catalysts are shown in Fig. 5. The particle size distribution obtained from the analysis of TEM images are also shown in Fig. 6. In agreement with the results of EXAFS measurement, the nano-sized Fe metal with a mean diameter (d) of *ca*. 8 nm having a narrow size distribution was found on the PAD-Fe/TiO_2-SiO_2 catalyst, whereas the aggregated Fe metal with various sizes are observed on img-Fe/TiO_2-SiO_2 catalyst (d = 23 nm).

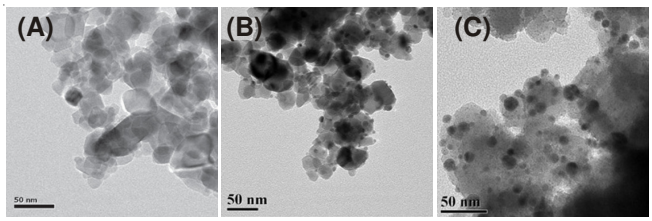

Fig. 5. TEM images of the TiO_2-SiO_2 (A), PAD-Fe-TiO_2-SiO_2 (B) and img- Fe-TiO_2-SiO_2 (C) catalyst after H_2 treatment at 473 K

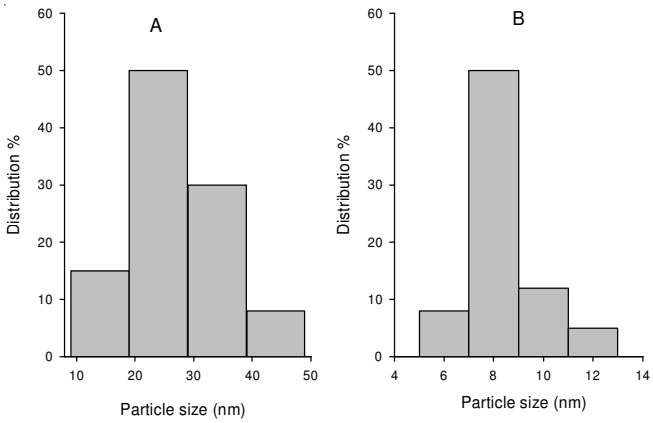

Fig. 6. Size distribution diagrams of Fe metal obtained from the TEM images of the img-Fe-TiO_2-SiO_2 (A) and PAD-Fe-TiO_2-SiO_2 (B) catalyst after H_2 treatment at 473 K

Photocatalytic reduction of Hg^{2+}: Fig. 7 displays the photocatalytic reduction of Hg^{2+} of 120 mg/L Hg^{2+} pertaining to (TiO_2-SiO_2, Img-Fe/TiO_2-SiO_2 and PAD-Fe/TiO_2-SiO_2) at solution pH 4 for different time intervals. It can be seen that the rate of Hg^{2+} photoreduction increased gradually with time reaching maximum efficiency values of 10, 64 and 100 % after 1 h with parent TiO_2-SiO_2, Img-Fe/TiO_2-SiO_2 and PAD-Fe/TiO_2-SiO_2 samples, respectively. The maximum photocatalytic reduction of Hg^{2+} was achieved in the case of PAD: Fe/ TiO_2-SiO_2 in which the band gap value is lower. The photocatalytic activities of the Fe-doped TiO_2-SiO_2 nanoparticles increased due to that Fe plays two important roles; lowering the energy of electron excitation from valance band to conduction band and hinders the rate of e^-/h^+ recombination Thus it lowered both the band gap (as confirmed from the UV-visible-DRS spectra analysis) and particle size (as confirmed from the TEM analysis). This resulted in increase in the surface area and pore volume and consequently showed the best photoactivity with Hg^{2+} reduction. Also, the adsorption experiments reveal that the adsorption efficiency % in case of TiO_2-SiO_2, Img-Fe/TiO_2-SiO_2 and PAD-Fe/TiO_2-SiO_2 is 9, 7 and 5 %, respectively. Therefore, in case of Img-Fe/TiO_2-SiO_2 and PAD-Fe/TiO_2-SiO_2, % of Hg^{2+} removal is photocatalytic reduction not adsorption process but in case of TiO_2-SiO_2, % of Hg^{2+} removal is adsorption not photocatalytic reduction.

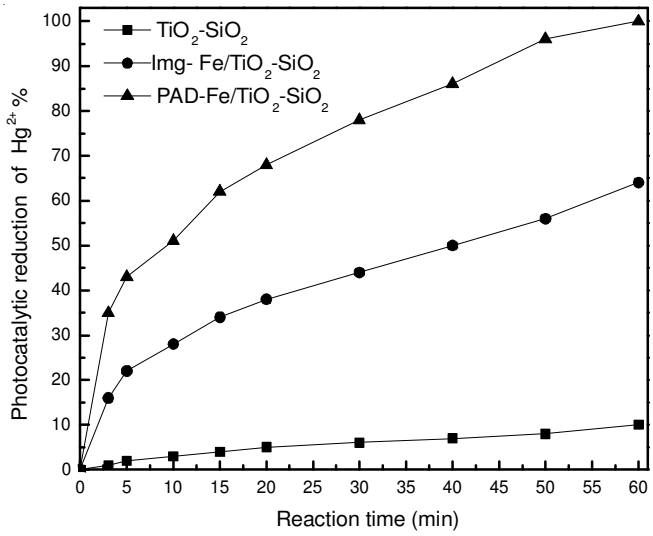

Fig. 7. Photocatalytic reduction of Hg^{2+}, % for TiO_2-SiO_2, img-Fe/TiO_2-SiO_2 and PAD-Fe/TiO_2-SiO_2

Conclusions

• It can be summarized that the nano-sized particles of Fe/TiO_2-SiO_2 can be prepared *via* two methods: photo-assisted deposition (PAD) and the conventional impregnation method. The characterization of such prepared catalysts by N_2 adsorption, XRD, UV-visible and XAFS techniques reveals the following remarks:

• The nano-sized Fe metal with a mean diameter (d) of *ca*. 8 nm having a narrow size distribution was found on the PAD-Fe/TiO_2-SiO_2 catalyst, whereas the aggregated Fe metal with various sizes are observed on img-Fe/TiO_2-SiO_2 catalyst (d = 23 nm).

• The calculated values of band gap for TiO_2-SiO_2, img-Fe/TiO_2-SiO_2 and PAD-Fe/TiO_2-SiO_2 are 3.20, 2.84 and 2.54, respectively.

• The surface area changed from 300 to 280 and 260 m^2/g in case of TiO_2-SiO_2, PAD-Fe/TiO_2-SiO_2 and img-Fe/TiO_2-SiO_2 respectively.

• The intensity of the Fe-Fe peak of the PAD-Fe-TiO_2-SiO_2 catalyst is smaller than the img-Fe/TiO_2-SiO_2 catalyst. These findings suggest that the size of Fe metal particles depends on the preparation method. Fe metal particles formed on the photo-deposited catalyst (PAD-Fe/TiO_2-SiO_2) shows smaller particle sizes than that obtained from the impregnated catalyst (img-Fe/TiO_2-SiO_2).

In summary, using the photo-assisted deposition method and TiO_2-SiO_2, nano sized Fe metal particles with a well-controlled size and a well dispersed state can be deposited on tetrahedrally coordinated Ti-oxide of the support. The direct interaction between nano-sized Fe metal and the photo-excited tetrahedrally coordinated Ti-oxide realized by the photo-assisted deposition method under UV-light irradiation have the possibility to design the unique and active nano-sized metal catalyst.

REFERENCES

1. E.M. Fournière, A.G. Leyva, E.A. Gautier and M.I. Litter, *Chemosphere*, **69**, 682 (2007).
2. J. Barron-Zambrano, S. Laborie, Ph. Viers, M. Rakib and G. Durand, *Desalination*, **144**, 201 (2002).
3. N. Serpone, Y.K. Ah-You, T.P. Tran, R. Harris, E. Pelizzetti and H. Hidaka, *Sol. Energy*, **39**, 491 (1987).
4. N. Serpone, E. Borgarello, E. Pelizzetti and M. Schiavello, Photocatalysis and Environment, Kluwer Academic Publishers, Dordrecht, p. 527 (1988).
5. A. Linsebigler, G. Lu and J.T. Yates, *Chem. Rev*., **95**, 735 (1995).
6. A. Fujishima, N.T. Rao and D.A. Rryk, *J. Photochem. Photobiol. C Rev.*, **1**, 1 (2000).
7. J.B. Christophe, A. Francine, C. Pascal, J. Marie and L. Frank, *Ceram. J. Am. Soc*., **80**, 3157 (1997).
8. Y. Zhu, L. Zhang, W. Yao and L. Cao, *Appl. Surf. Sci*., **158**, 32 (2000).
9. P.T. Tanev, M. Chibwe and T.J. Pinnavaia, *Nature*, **368**, 321 (1994).
10. J.V. Walker, M. Morey, H. Carlsson, A. Davidson, G.D. Stucky and A.J. Butler, *J. Am. Chem. Soc*., **119**, 6921 (1997).
11. A.J. Anderson and A.J. Bard, *Phys. J. Chem*., **99**, 9882 (1995).
12. S.A. Ruetten and J.K. Thomas, *Photochem. Photobiol. Sci*., **2**, 1018 (2003).
13. H. Chun, Y. Wang and H. Tang, *Appl. Catal. B*, **30**, 277 (2001).
14. C.Y. Wang, C.Y. Liu and X. Zheng, *Colloids Surf. A*, **131**, 271 (1998).
15. J.C. Yang, Y.C. Kim and Y.G. Shul, *Appl. Surf. Sci*., **121**, 525 (1997).
16. L. Zhu, Z.-D. Meng, C.-Y. Park, J.-G. Choi, T. Ghosh and W.-C. Oh, *Asian J. Chem.*, **24**, 4191 (2012).
17. F.B. Li and X.Z. Li, *Appl. Catal. A*, **228**, 15 (2002).
18. K. Mori, T. Hara, T. Mizugaki, K. Ebitani and K. Kaneda, *J. Am. Chem. Soc.*, **126**, 10657 (2004).
19. A. Fukuoka, H. Araki, J. Kimura, Y. Sakamoto, T. Higuachi, N. Sugimoto, S. Inagaki and M. Ichikawa, *J. Mater. Chem.*, **14**, 752 (2004).
20. F. Boccuzzi, A. Chiorino, M. Manzoli, P. Lu, T. Akita, S. Ichikawa and M. Haruta, *J. Catal.*, **202**, 256 (2002).
21. M. Anpo and J.M. Thomas, *Chem. Commun.*, 3273 (2006).
22. H. Yamashita and M. Anpo, *Curr. Opin. Solid State Mater. Sci.*, **7**, 471 (2004).
23. M. Anpo and M. Che, *Adv. Catal.*, **44**, 119 (1999).
24. H. Yamashita, K. Ikeue, T. Takewaki and M. Anpo, *Topics Catal.*, **18**, 95 (2002).
25. K. Ikeue, H. Yamashita, T. Takewaki and M. Anpo, *J. Phys. Chem. B*, **201**, 8350 (2001).
26. M.Anpo, H.Yamashita, Y. Ichihashi, Y. Fujii and M. Honda, *J. Phys. Chem. B*, **101**, 2632 (1997).
27. M. Anpo, H. Yamashita, Y. Ichihashi, M. Anpo, M. Hasimoto, C. Louis and M. Che, *J. Phys. Chem.*, **100**, 16041(1996).
28. H. Yamashita, K. Yoshizawa, M. Ariyuki, S. Higashimoto, M. Che and M. Anpo, *Chem. Commun.*, 435 (2001).
29. C. Murata, H. Yoshida and T. Hattori, *Chem. Commun.*, 2412 (2001).
30. F. Amano, T. Yamaguchi and T. Tanaka, *J. Phys. Chem. B*, **109**, 281 (2006).
31. N. Ichikuni, H. Murayama, K.K. Bando, S. Shimazu and T. Uematsu, *Anal. Sci.*, **17**, 1193 (2001).
32. G. Lassaleta, A. Fernaandez, J.P. Espinoos and A.R. Gonzaolez-Elipe, *J. Phys. Chem*., **99**, 1848 (1995).
33. M. Schiavello, Heterogeneous Photocatalysis, Wiley, Chichester (1997).
34. R.J. Davis and Z. Liu, *Chem. Mater*., **9**, 2311 (1997).
35. D.F. Ollis, *Catal. Technol.*, **2**, 149 (1998).
36. K. Kosuge and S. Singh, *J. Phys. Chem. B*, **18**, 3563 (1999).
37. A.A. Belhekar, S.V. Awate and R. Anand, *Catal. Commun*., **3**, 453 (2002).
38. B.J. Aronson, C.F. Blanford and A. Stein, *Chem. Mater*., **9**, 2842 (1997).
39. S. Cheng, S. Tsai and Y. Lee, *Catal. Today*, **26**, 87 (1995).
40. T.E. Alcacio, D. Hesterberg, J.W. Chou, J.D. Martin, S. Beauchemin and D.E. Sayers, *Geochim. Cosmochim. Acta*, **65**, 1355 (2001).